© 2016. Published by The Company of Biologists Ltd | Development (2016) 143, 4203-4213 doi:10.1242/dev.138289

RESEARCH ARTICLE

A new mode of mitochondrial transport and polarized sorting regulated by Dynein, Milton and Miro

Anna Melkov, Raju Baskar, Yehonatan Alcalay and Uri Abdu*

ABSTRACT

Intrinsic cell microtubule (MT) polarity, together with molecular motors and adaptor proteins, determines mitochondrial polarized targeting and MT-dependent transport. In polarized cells, such as neurons, mitochondrial mobility and transport require the regulation of kinesin and dynein by two adaptor proteins, Milton and Miro. Recently, we found that *dynein heavy chain 64C* (*Dhc64C*) is the primary motor protein for both anterograde and retrograde transport of mitochondria in the *Drosophila* bristle. In this study, we show that a molecular lesion in the *Dhc64C* allele that reduced bristle mitochondrial velocity generated a variant that acts as a 'slow' dynein in an MT-gliding assay, indicating that dynein directly regulates mitochondrial transport. We also showed that in *milton-RNAi* flies, mitochondrial flux into the bristle shaft, but not velocity, was significantly reduced. Surprisingly, mitochondria retrograde flux, but not net velocity, was significantly decreased in *miro-RNAi* flies. We thus reveal a new mode of mitochondrial sorting in polarized cell growth, whereby bi-directional mitochondrial transport undertaken exclusively by dynein is regulated by Milton in the anterograde direction and by a Miro-dependent switch to the retrograde direction.

KEY WORDS: Bristle, *Drosophila*, Dynein, Milton, Miro, Mitochondria

INTRODUCTION

Owing to their roles in ATP production, calcium homeostasis and cell signaling, mitochondria are essential for cellular function and they form a dynamic network within the cell. In highly polarized cells, such as neurons, long-distance transport of mitochondria relies mainly on microtubules (MTs), which ensure the appropriate distribution of the mitochondrial network – a process that is also essential for proper cell function. In neurons of both vertebrates and invertebrates, axonal MTs display a uniform orientation, with their plus-ends facing the axon tip (Baas et al., 1988; Stone et al., 2008). In vertebrate dendrites, MTs present mixed polarity, with equal numbers of plus- and minus-end-out MTs (Baas et al., 1988). However, in invertebrate dendrites, the majority of MTs show uniform polarity, with the minus-ends pointing away from the cell body (Stone et al., 2008). The same is true for *Drosophila* bristle cells: MT-based mitochondrial transport relies on the plus-end-directed motor protein Kinesin-1, and the minus-end-directed motor cytoplasmic Dynein-1. In both axons and dendrites, the direction of mitochondrial transport depends on MT polarity (reviewed in Schwarz, 2013).

Motor-based transport of mitochondria is mediated through the actions of several motor-associated adaptor proteins and mitochondrial scaffolding proteins. In *Drosophila*, the mitochondria adaptor protein Milton is required for kinesin-mediated transport of mitochondria to nerve terminals (Stowers et al., 2002), to photoreceptors (Gorska-Andrzejak et al., 2003) and along the axon (Glater et al., 2006). In mammalian cells, TRAK1 and TRAK2, homologs of the *Drosophila* Milton protein, are required for the mobility of mitochondria along the axons of hippocampal neurons (Koutsopoulos et al., 2010) and for steering mitochondria to axons and dendrites (van Spronsen et al., 2013). Miro, another mitochondrial motor-adaptor protein, is an atypical mitochondrial GTPase (Fransson et al., 2003), which is required for the transport of mitochondria in *Drosophila* (Guo et al., 2005) and in mammalian cells (Fransson et al., 2006). It was further demonstrated that Miro forms a complex with Milton and the motor protein Kinesin-1 (Glater et al., 2006) and could directly bind to Kinesin heavy chain (Khc) in a Ca^{2+}-dependent manner (Macaskill et al., 2009; Saotome et al., 2008; Wang and Schwarz, 2009).

The highly polarized *Drosophila* bristle cell represents a unique, dendrite-like cell in which stable MTs are uniformly oriented with their minus-ends pointed toward the bristle tip (Bitan et al., 2012). Thus, in the context of the bristle cell, anterograde transport is defined as MT-minus-end-oriented (i.e. towards the bristle tip) and retrograde transport is defined as MT-plus-end-oriented (i.e. towards the bristle cell base). We have studied the role of MT motor proteins in mitochondrial long-distance transport in bristle cells and found that in *Dynein heavy chain* (*Dhc64C*) mutant bristles, the net velocity of mitochondrial movement in both the anterograde and the retrograde directions was significantly reduced, whereas in *Khc* mutants, such movement was significantly higher (Melkov et al., 2015). These results suggest that Dhc64C is the primary motor for both anterograde and retrograde fast mitochondria transport, whereas Khc provides a competing force to Dhc64C (Melkov et al., 2015).

To better understand the role of bristle mitochondrial transport, we focused our attention in the present study to the genetic, molecular and biochemical characterization of *Dhc64C* mutants. We found that mutations in *Dhc64C* affected bristle morphology and MT and actin organization. We reveal the molecular lesions in three *Dhc64C* alleles and showed that one of these alleles acts as a 'slow' version of dynein in an MT-gliding assay. Surprisingly, examination of the function of two broadly known mitochondrial adaptor proteins, Miro and Milton, showed different roles for each. We found that Miro is preferentially needed for retrograde mitochondrial (i.e. MT plus-end-directed) transport. At the same time, Milton was shown to be responsible for primary polarized mitochondria sorting into the developing bristle cell.

RESULTS

Identification of *Dhc64C* alleles that affect actin and the MT network during bristle development

The following loss-of-function alleles were used in our study: $Dhc64C^{4-19}$, $Dhc64C^{902}$, $Dhc64C^{3-2}$, $Dhc64C^{6-6}$, $Dhc64C^{6-12}$, $Dhc64C^{6-10}$ and $Dhc64C^{8-1}$. Whereas $Dhc64C^{4-19}$ (Gepner et al., 1996) and $Dhc64C^{902}$ (Li et al., 2008) were reported to be amorphic

Department of Life Sciences, Ben-Gurion University of the Negev, Beer-Sheva 8410500, Israel.

*Author for correspondence (abdu@bgu.ac.il)

U.A., 0000-0003-1226-0750

Received 4 April 2016; Accepted 23 September 2016

Development (2016) 143, 4203-4213 doi:10.1242/dev.138289

alleles, and $Dhc64C^{6-6}$, $Dhc64C^{6-12}$ and $Dhc64C^{6-10}$ (Gepner et al., 1996) were reported to be hypomorphic alleles, the nature of the $Dhc64C^{8-1}$ and $Dhc64C^{3-2}$ alleles remained unknown. We therefore first analyzed the lethality of each of the above alleles in combination with a deficiency that removed the 64B13-64C4 region [Df(3L) Exel6102], which included the *Dhc64C* gene. We found that whereas $Dhc64C^{4-19}$, $Dhc64C^{902}$ and $Dhc64C^{3-2}$ hemizygotes were lethal, $Dhc64C^{6-12}$, $Dhc64C^{8-1}$, $Dhc64C^{6-10}$ and $Dhc64C^{6-6}$ hemizygotes were viable. However, the affected flies died 4-5 days after eclosion. Based on their viability, we refer to the lethal hemizygous as amorphic alleles and the viable alleles as hypomorphic alleles. Of the hemizygous viable alleles, $Dhc64C^{8-1}$, $Dhc64C^{6-10}$ and $Dhc64C^{6-6}$ but not $Dhc64C^{6-12}$ presented bristle defects.

Examination of mutant bristles using scanning electron microscopy (SEM) showed these entities to be much shorter than wild-type bristles (Fig. 1). Specifically, measuring the lengths of adult posterior scutellar bristles revealed a mean (±s.d.) length of 213±24 µm (n=6) in *Dhc64C* mutants, a value that was significantly shorter ($F_{1,17}$=353.7, P<0.001) than that in wild-type bristles [339± 26 µm (n=15)]. Moreover, closer examination of bristle morphology (Fig. 1B-D) revealed that the upper part (i.e. the first third) of the bristle was very thin and highly twisted (Fig. 1C), and lacked the cuticular structure of ridges and valleys, compared with wild-type bristles (Fig. 1A). The lower part of the bristle closest to the base was wider in the mutant than it was in the wild type and more than 50% of the mutant bristles presented an ectopic extension at the bristle base with a growth direction almost opposite to the main bristle extension (arrows in Fig. 1B,D). Next, rescue experiments were performed to test whether the expression of transgenes encoding HA-*Dhc64C* (Silvanovich et al., 2003) could rescue the bristle defects found in the *Dhc64C* hemizygous mutant. We found full rescue of bristle length and no ectopic extension at the bristle base, meaning that the mutation in *Dhc64C* was responsible for the observed defects. Next, we analyzed the organization of the actin cytoskeleton during pupal development. Phalloidin staining of actin bundles, along with staining of the bristle shaft membrane with antibodies against Dusky-like protein (Dyl) (Fernandes et al., 2010; Nagaraj and Adler, 2012), revealed that in *Dhc64C* mutant bristles, actin bundles were disorganized in the lower areas of the bristle shaft (Fig. 2D,F,F′). Indeed, digital cross-sections through mutant bristles demonstrated that whereas in wild-type bristles the actin bundles were restricted to the shaft membrane (Fig. 2C′), in *Dhc64C* mutants, actin bundles were no longer found at the membrane but instead were distributed throughout the bristle cytoplasm (Fig. 2F′). Next, we compared thin transverse sections of bristles from wild type (Fig. 2G,G′; 10 bristles from 3 pupae) and *Dhc64C* mutants (Fig. 2H,H′; 13 bristles from 3 pupae) 42-48 h after puparium formation (APF), using transmission electron microscopy (TEM). Such analysis revealed that actin bundles could be seen both at the cell membrane and in the bristle shaft in $Dhc64C^{8-1}$ hemizygotes (arrows in Fig. 2H,H′; in all tested bristles), whereas the triangular actin bundles observed in the wild-type bristles were attached to the shaft membrane (red arrows in Fig. 2G,G′). Closer examination of the membrane-bound actin bundles in the mutant (thin black arrows in Fig. 2H,H′) showed them to be much smaller than those in the wild type, with half of the bundles in the mutant being triangular and the other half presenting irregular shapes (red arrows in Fig. 2H,H′). These results corroborate with the actin staining seen in the confocal microscopy study, suggesting that mutations in *Dhc64C* strongly affect actin organization during bristle development.

Next, we considered the organization of MTs in *Dhc64C* mutant bristles. To analyze MT organization, developing bristles were stained with antibodies against acetylated tubulin, which stained the stable population of MTs (Fig. 3A-F). In the wild type, acetylated tubulin was abundant along the entire shaft (Fig. 3B-B‴). In *Dhc64C* mutants, MTs were evenly distributed in the lower part of the bristle, (Fig. 3E′); however, from the middle of the developing bristle (Fig. 3E″), the MTs were disorganized, with MT-absent areas appearing, as revealed by digital cross-section analysis (Fig. 3E‴). The areas lacking MTs expanded gradually towards the bristle tip (Fig. 3E‴). Such defects in MT organization were also detected in all three hemizygous alleles studied using confocal microscopy.

As described above, whereas the lower part of the *Dhc64C* mutant bristle contained MTs, a decrease in MT density from the middle part to the tip of the bristle shaft was noted. Closer examination of MT organization by TEM revealed, as described

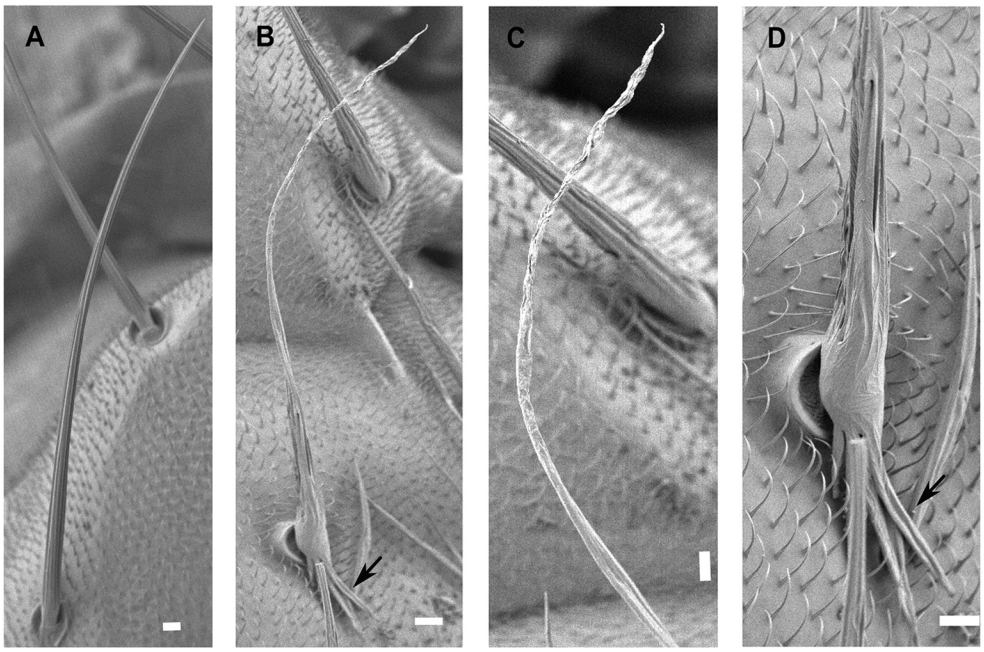

Fig. 1. Mutations in *Dhc64C* affect bristle development. Scanning electron micrographs of adult bristles from (A) wild-type flies, (B) transheterozygote $Dhc64C^{4-19}/Dhc64C^{8-1}$ flies showing severe morphological defects and overall bristle length decrease (black arrow indicates the ectopic extension at the base of the cell), (C) transheterozygote $Dhc64C^{4-19}/Dhc64C^{8-1}$ flies showing high magnification of a major defect in the grooved surface of the tip bristle area, (D) transheterozygote $Dhc64C^{4-19}/Dhc64C^{8-1}$ flies showing high magnification of bristle base area with ectopic extension marked with a black arrow. Scale bars: 10 µm.

Development (2016) 143, 4203-4213 doi:10.1242/dev.138289

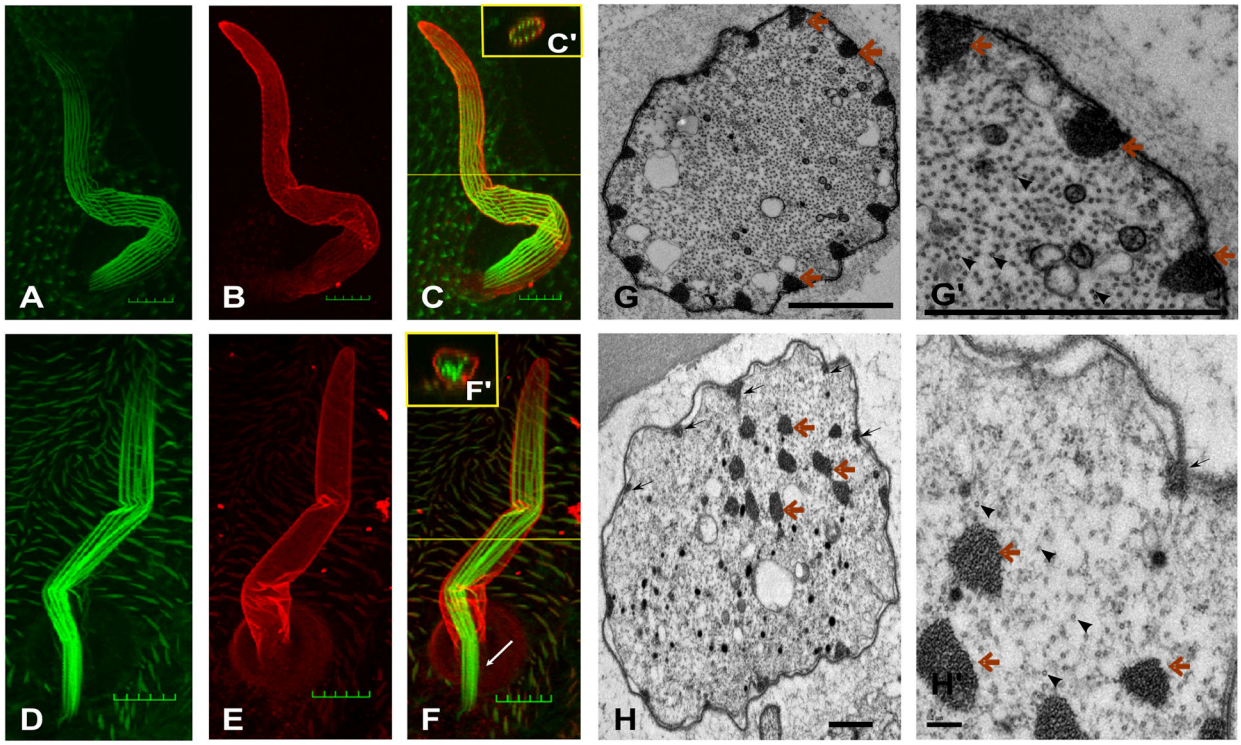

Fig. 2. Defects in actin organization in *Dhc64C* mutant bristles. (A-F) Confocal projections of elongating bristles from wild-type (A-C) and *Dhc64C*$^{8-1}$ hemizygous pupae (D-F). In A,D, actin is green; in B,E, Dusky-like (Dyl) is red; C,F, merged images. In the wild type, actin bundles are associated with the cell membrane. In *Dhc64C*$^{8-1}$ flies, actin bundles are found in the bristle cytoplasm. C′ and F′ are transverse digital sections through the bristle shaft. Whereas actin bundles were found in the ectopic extension at the bristle base, the membrane marker Dyl was not found at the membrane of this extension (white arrow in F). Scale bar: 10 µm. (G,H) TEM images of thin transverse sections through a macrochaetae from wild type (G,G′) and *Dhc64C*$^{8-1}$ hemizygous pupae (H,H′). In the wild type, triangular-shaped actin bundles are attached to the cell membrane (red arrows in G,G′). In *Dhc64C*$^{8-1}$ flies, hemizygous macrochaetae actin bundles could be seen at the cell membrane (black arrows in H,H′) and in the bristle shaft (red arrows in H-H′). The membrane-bound actin bundles were much smaller than those seen in the wild type. MTs in the WT (arrowheads in G′) and the *Dhc64C* mutant (arrowheads in H′) fill the cytoplasm. Scale bars: 2 µm (G,G′), 1 µm (H) and 200 nm (H′).

before (Tilney et al., 2000), that in the WT (10 bristles from 3 pupae were analyzed), the bristle cytoplasm contains a large population of MTs (Fig. 3G and arrows in Fig. 3H). However, in *Dhc64C* mutants (10 bristles from 3 pupae were analyzed), we found that whereas in five of the analyzed sections MTs were found in the cytoplasm (Fig. 3I, and arrows in Fig. 3J), in the rest of the bristles analyzed, we detected large white areas lacking any organelles (arrowheads in Fig. 3K). Indeed, closer examination of these sections revealed that the entire cytoplasm lacked MTs (Fig. 3L). We believe that sections from *Dhc64C* mutants bristle, which contain MTs, may represent the lower part of the bristle and the section without MTs may represent the middle to the upper parts of the bristle.

Dhc64C$^{8-1}$ allele is a ‘slow’ dynein mutant

Of the known EMS-induced *Dhc64C* alleles, only the lesion in *Dhc64C*^{902} has been characterized. Here, a premature stop codon, which results in a truncated product at amino acid 1173, was introduced (Horne-Badovinac and Bilder, 2008). In the present study, we identified the nature of the lesion in *Dhc64C*$^{8-1}$, *Dhc64C*$^{6-6}$ and *Dhc64C*$^{6-10}$ by sequencing the *Dhc64C* gene from genomic DNA derived from hemizygous flies. We found that the *Dhc64C*$^{8-1}$ allele contained a specific transversion mutation (A to T), which resulted in an amino acid change, namely D1922V. Closer examination revealed that the original Asp was conserved from yeast to humans (Box 1 in Fig. 4). We further found that *Dhc64C*$^{6-6}$ and *Dhc64C*$^{6-10}$ share a common transition mutation (T to C), which also resulted in an amino acid change, namely W1527R (Box 2 in Fig. 4). This tryptophan too was conserved from yeast to humans. Moreover, we demonstrated that *Dhc64C*$^{6-6}$ contained another specific transversion mutation (G to T) that results in an amino acid change, namely G1147C, with the glycine also being conserved in humans (Box 3 in Fig. 4). The overall structure of the dynein heavy chain is divided into four domains, specifically the tail, which is the cargo-binding domain, the head (motor), which is the site of ATP hydrolysis, the linker, which is the mechanical amplifier, and the stalk, which is the microtubule-binding domain (Fig. 4; Kikkawa, 2013). Closer examination revealed that the aspartic acid at position 1922 that was changed to valine (D1922V) in *Dhc64C*$^{8-1}$ is found within the AAA1 domain (Fig. 4A). This residue corresponds to D1933 in human DYNC1H1. We subsequently examined the effect of this amino acid change as found in the *Dhc64C*$^{8-1}$ allele in an MT-gliding assay using human DYNC1H1. Since the aspartic acid at position 1922 is highly conserved among cytoplasmic dynein sequences from yeast to humans, we introduced this point mutation into human DYNC1H1 (at the corresponding D1933 position) to produce a fully recombinant human dynein complex (called DYNC1H1$^{D/V}$, hereafter), as previously described (Schlager et al., 2014), using insect cells. Size exclusion chromatography profiles of wild-type dynein complex and DYNC1H1$^{D/V}$ revealed that the latter eluted as a single peak at the same elution time as the wild-type protein (Fig. 4B). Subsequent SDS-PAGE analysis revealed that all six dynein subunits were present in both complexes (Fig. 4C). Next, we found that in the wild-type dynein, the mean gliding speed per MT was 0.163±0.050 µm/s (n=27; Fig. 4D,E,H; Movie 1); however, in the mutant DYNC1H1$^{D/V}$, the mean MT gliding speed of 0.023±0.007 µm/s (n=114; Fig. 4F,G,I; Movie 2) was

Development (2016) 143, 4203-4213 doi:10.1242/dev.138289

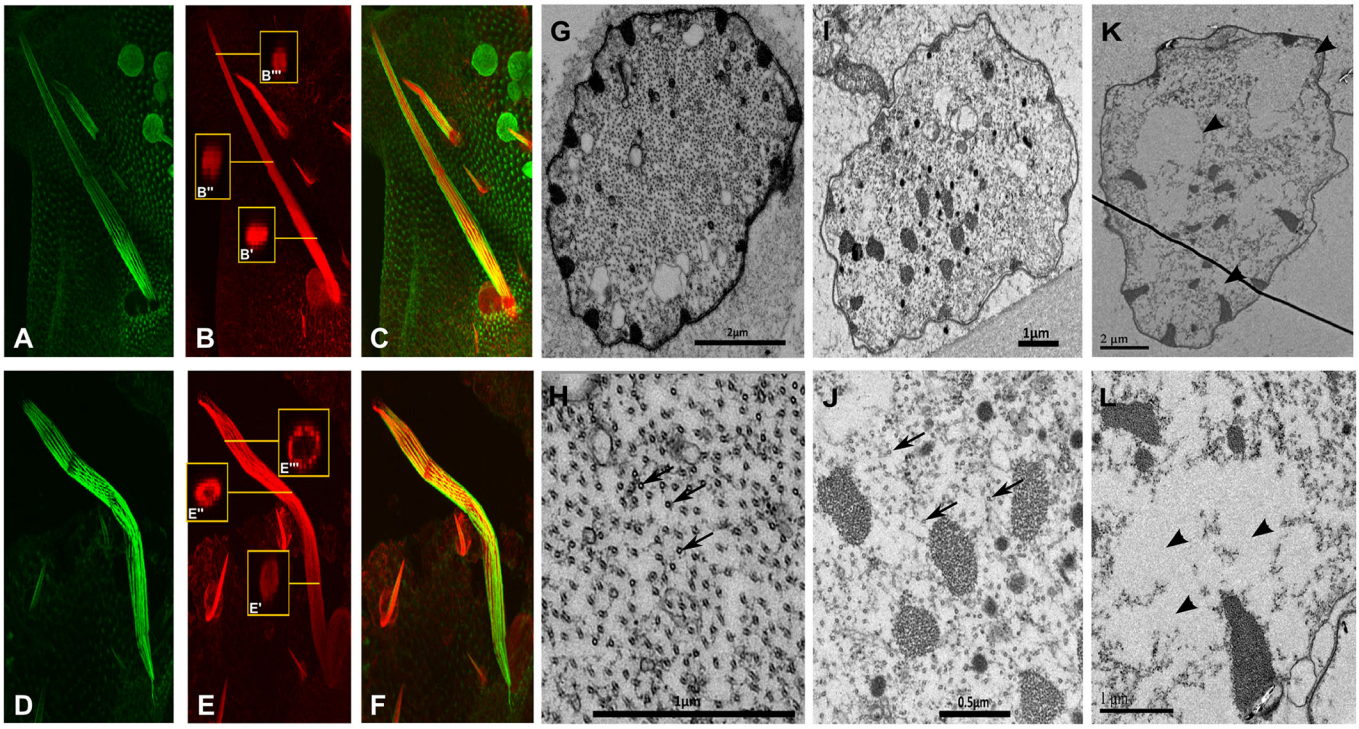

Fig. 3. Defects in microtubule organization in *Dhc64C* mutant bristles. (A-F) Confocal projections of elongated bristles from wild-type (A-C) and *Dhc64C*$^{8-1}$ hemizygous pupae (D-F). In A,D actin is stained with Phalloidin in green; in B,E, acetylated tubulin is red; C,F, merged images. In the wild type, stable MTs were found throughout the bristle cytoplasm as revealed by transverse digital sectioning (B′-B‴). In *Dhc64C*$^{8-1}$ flies, MTs were found in the lower third of the shaft (E′), whereas in the middle cell area, MTs were irregularly distributed, with areas void of MTs (E″). These MT-lacking areas gradually expanded towards the bristle tip (E‴). TEM of thin transverse sections through a macrochaetae from WT (G-H) and *Dhc64C*$^{8-1}$ mutants (I-L). (K) In the wild type, MTs fill the bristle shaft (G, and arrows in H). In *Dhc64C*$^{8-1}$ mutants, in several of the thin sections MTs are found at the bristle shaft (I and arrows in J) and in other sections, there are areas that lack MTs (K and arrowheads in L).

significantly slower ($F_{1,132}$=711.59, P<0.001). These results suggest that changing the aspartic acid at position 1933 (corresponding to *Drosophila* D1922), found at the first AAA+ domain, to valine reduced dynein velocity *in vitro*, probably because of a direct effect on its motor function rather than defects in dynein complex assembly. These results demonstrate that the *Dhc64C*$^{8-1}$ allele is a 'slow' Dhc mutant.

Regulation of Dhc64C mitochondrial transport is not dependent on the p150^{Glued} dynactin subunit

Having previously shown that dynein is the primary motor protein involved in antero- and retrograde mitochondrial transport (Melkov et al., 2015), we now considered the role of dynein accessory proteins involved in integrated regulation of transport driven by dynein. Dynactin, a dynein activator, is a multi-subunit protein complex that is required for most, if not all, types of cytoplasmic dynein activity in eukaryotes (reviewed in Kardon and Vale, 2009). Dynactin comprises 11 different subunits, including the filament of actin-related protein 1 (Arp1) and the largest subunit, p150 (reviewed in Schroer, 2004). In *Drosophila*, the *Glued* (*Gl*) gene (*DCTN1-p150*) encodes the homolog of the p150 subunit of the vertebrate dynactin complex (Gill et al., 1991; Holzbaur et al., 1991; Swaroop et al., 1987). To study the function of Glued in bristle development and mitochondrial transport, we specifically reduced Glued levels in the bristle using RNAi or by expressing the dominant-negative form of Glued (*Glued-DN*), containing only the N-terminal 922 amino acids (Allen et al., 1999; Bielska et al., 2014) using the UAS/Gal4 system. *Glued-RNAi* (12 flies; 48 bristles were tested) and *Glued-DN* (3 flies; 12 bristles were tested) flies were viable, yet showed defects in bristle morphology in all tested animals, with the upper part of the bristle being thin and twisted (Fig. 5B-D) compared with wild-type bristles (Fig. 5A). Since both actin and MT network organization was severely affected in *Dhc64C* mutants bristles (Figs 2,3), we examined the organization of these cytoskeletal components in the bristles of *Glued-RNAi* and *Glued-DN* flies. Surprisingly, defects in neither MT nor actin distribution were detected in bristles from *Glued-DN* flies (Fig. S1D-F).

To test whether Dhc64C mitochondrial transport function was dependent on p150^{Glued}, we quantified mitochondrial transport parameters in the bristles of *Glued-DN* mutant flies. We found that there were no obvious defects in mitochondrial distribution in bristle cells of *Glued-DN* flies (Fig. 5F; Movie 4), compared with wild-type cells (Fig. 5E; Movie 3). We also found that there were no defects in the net velocity of anterograde (2.39±2.32 µm/s) and retrograde (2.18±1.66 µm/s) mitochondrial movement (Table 1). However, a significant shift (P=0.028) in the direction of movement was detected in the bristles of *Glued-DN* mutant flies, with 88.06±15.25% of all dynamic mitochondria moving in the anterograde direction and only 11.94±15.25% moving in the retrograde direction (Table 1; Fig. 5H). In wild-type bristles, 72±19.45% of the measured movement occurred in the anterograde direction and 28±19.45% of the measured movement was in the retrograde direction (Melkov et al., 2015; Table 1; Fig. 5G). We also measured the flux of mitochondrial transport [i.e. the number of mitochondrial movements per unit time (100 s) per unit area (100 µm^2)] and found that in *Glued-DN* flies, there was a significant reduction (P<0.001) in the retrograde flux to 0.24±0.29, but not anterograde flux (2.74±

Development (2016) 143, 4203-4213 doi:10.1242/dev.138289

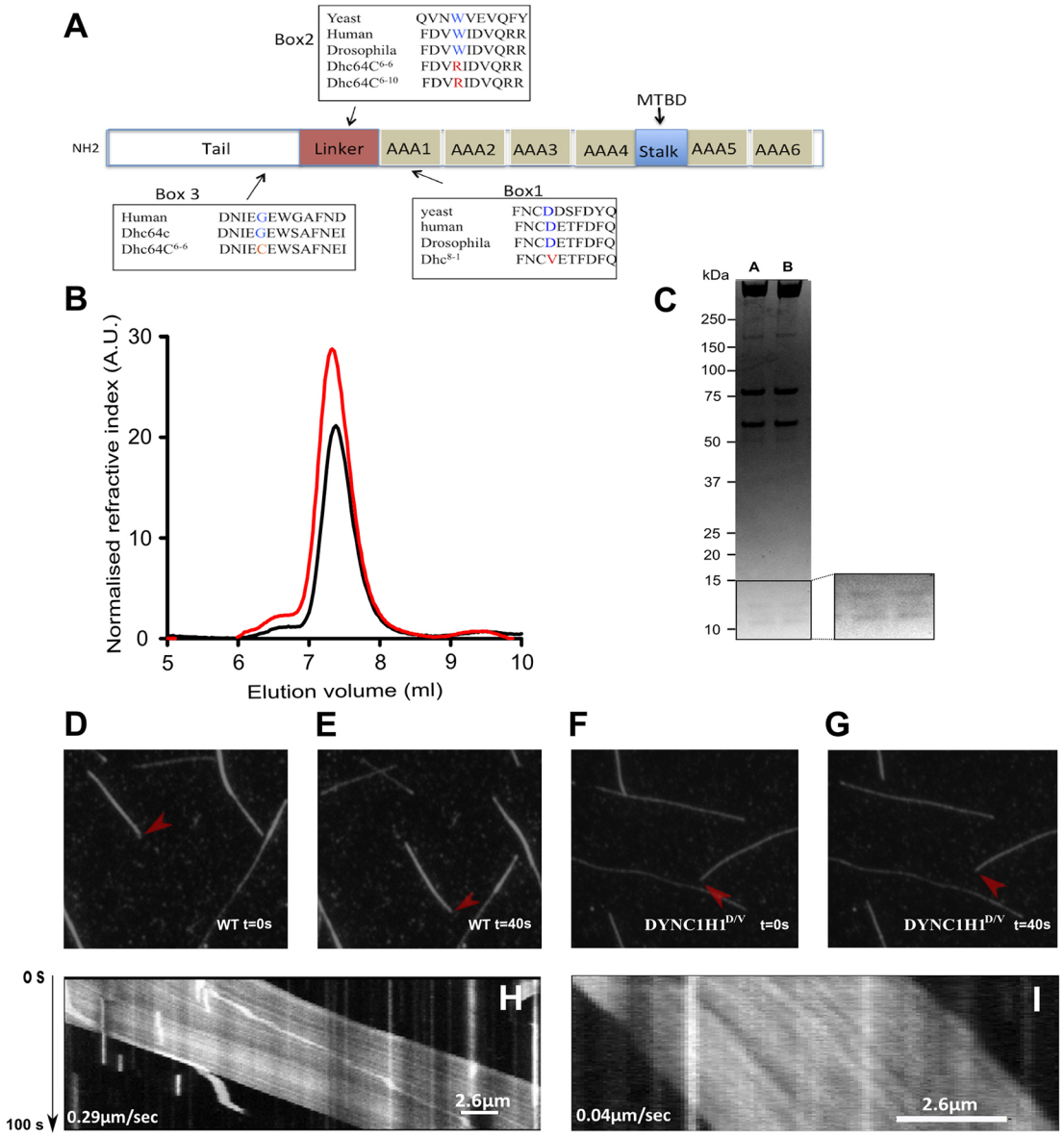

Fig. 4. Identification of the nature of the genetic lesion in *Dhc64C*$^{8-1}$, *Dhc64C*$^{6-6}$ and *Dhc64C*$^{6-10}$ alleles. (A) Schematic showing the overall structure of the dynein heavy chain protein. The protein is divided into four domains, namely the tail, which is the cargo-binding domain, the head (motor), which is the site of ATP hydrolysis (containing six AAA+ domains), the linker, which is the mechanical amplifier, and the stalk, which is the microtubule-binding domain (MTBD). In the *Dhc64C*$^{8-1}$ allele, a D1922V change was noted, with this residue being found in the first AAA+ domain. This Asp is conserved from yeast to *Drosophila* (box 1). In the *Dhc64C*$^{6-6}$ and *Dhc64C*$^{6-10}$ alleles, a W1527R change was detected, with this residue being found in the linker domain. This Trp is also conserved from yeast to *Drosophila* (box 2). Another mutation was found in the *Dhc64C*$^{6-6}$ allele, leading to a G1147C change, with this residue being found in the tail domain and conserved from yeast to humans (box 3). (B) Size-exclusion chromatography traces for the wild-type recombinant dynein complex (red) and mutant recombinant dynein complex (DYNC1H1$^{D/V}$) (black). Both complexes eluted at the same volume. (C) Coomassie Blue-stained SDS-PAGE of the purified recombinant dynein complex. The inset highlights the 10-15 kDa range from a gel with better low molecular mass separation in which bands corresponding to the different light chains can be discriminated. All dynein complex subunits are present in the wild-type (lane A) and DYNC1H1$^{D/V}$ complexes (lane B). (D-G) Stills from an MT-gliding assay with immobilized recombinant human dynein. D,E, wild-type recombinant dynein complex; F,G, DYNC1H1$^{D/V}$ recombinant human dynein. In D,F, t_1=0; in E,G, t_2=40 s. Red arrowheads mark the ends of the MTs. The gliding distance was much smaller with DYNC1H1$^{D/V}$ than with the wild type. (H,I) Representative kymograph of wild-type DYNC1H1 complex (H) and mutant DYNC1H1$^{D/V}$ complex (I). Time is on the *y*-axis, with the vertical bar indicating 100 s. The calculated gliding MT velocities are shown in each kymograph.

1.84), compared with wild type, where retrograde mitochondria flux was 0.92±0.68 and anterograde flux was 2.39±1.45 (Table 1).

milton is required for polarized sorting of mitochondria into bristle cells

Since it was shown that motor-based transport of mitochondria is mediated through the action of several adaptor proteins, we analyzed the functions of two well-known mitochondrial adaptor proteins, Milton and Miro. To study the function of Milton in mitochondrial transport, we specifically reduced *milton* levels in the bristle by RNAi, using the UAS/Gal4 system. We found that *milton-RNAi* flies were viable, with no obvious defects in bristle morphology in all tested animals (Fig. 6A; 4 flies, 16 bristles were tested). However, upon following mitochondrial mobility in the mutant flies, we noted defects in polarized sorting of mitochondria into bristle cells. We found that early in bristle

Development (2016) 143, 4203-4213 doi:10.1242/dev.138289

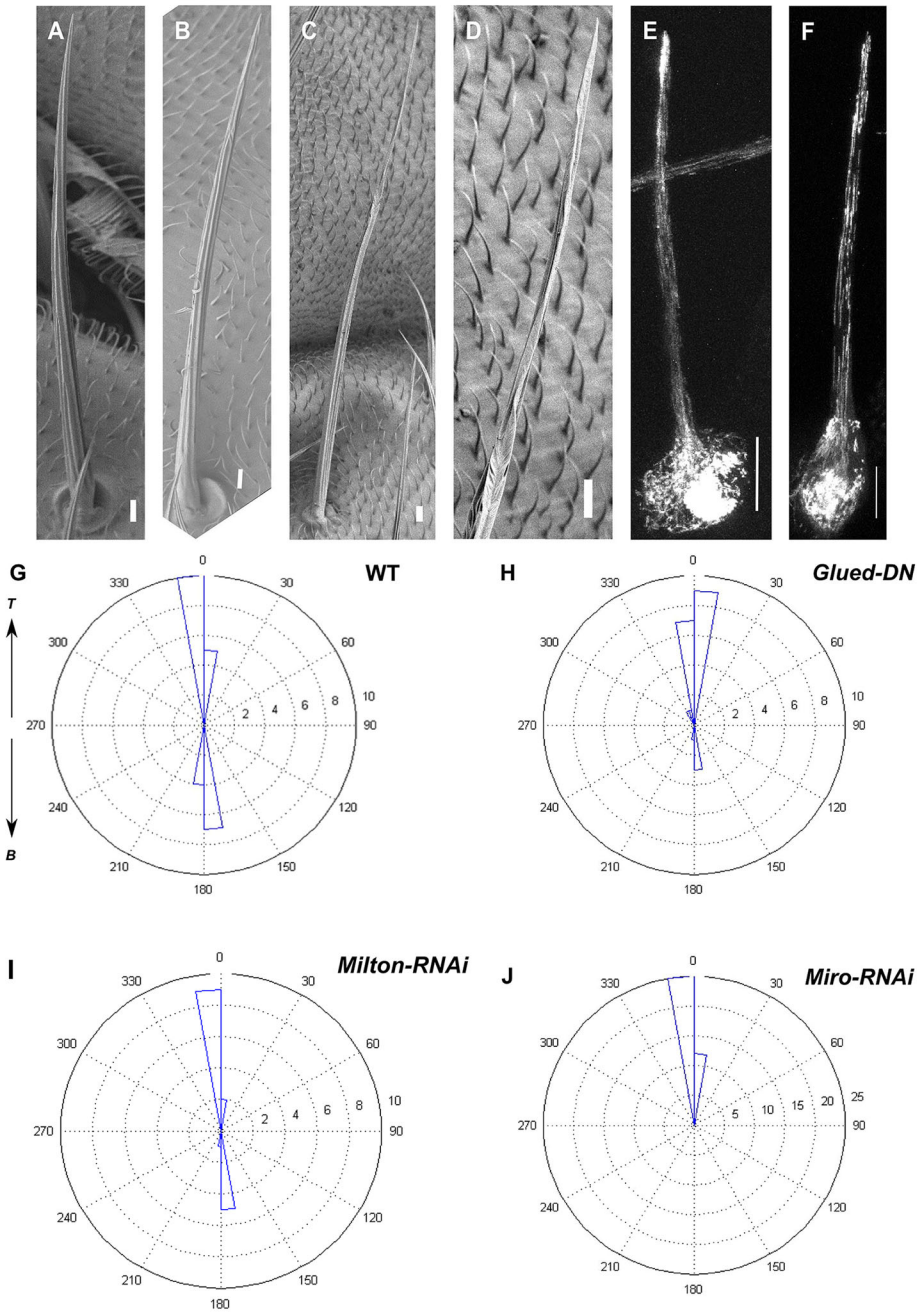

Fig. 5. Mutations in *Glued* affect bristle morphology. SEM images of adult bristles from (A) wild-type, (B) *neur-Gal4-UAS-p150-RNAi*, (C) *neur-Gal4-UAS-p150-delta96B* and (D) *UAS-p150-delta96B* flies. D is a higher magnification image of the tip area, showing defects in the characteristic parallel surface groove morphology. (E) Confocal projections from the developing bristle in a wild-type fly expressing *UAS-Mito-GFP* shows evenly distributed mitochondria throughout entire bristle cell. (F) Confocal projections from the developing bristle in a *neur-Gal4-UAS-p150-delta96B* fly expressing *UAS-Mito-GFP* shows no visible defects in the mitochondrial localization pattern. (G-J) Representative circular rose diagrams representing the directionality of mitochondrial movement in *neur-UAS-Mito-GFP* (G), *neur-Gal4-UAS-p150-delta96B; Mito-GFP* (H), *neur-Gal4-UAS-Milton-RNAi*^{44477}; *Mito-GFP* (I) and *UAS-miro-RNAi*^{106683}; *Mito-GFP* (J). The diagrams show frequency of mitochondrial movement in a certain orientation. Diagrams are oriented as follows: T, movement towards the tip of bristle shaft (anterograde direction); B, movement towards the base of bristle shaft (retrograde direction). (G) In *neur-UAS-Mito-GFP*, total number of mitochondrial movements measured=26, anterograde=15 and retrograde=11. (H) In *neur-Gal4-UAS-p150-delta96B*, total number of mitochondrial movements=22, anterograde=18 and retrograde=4. (I) In *neur-Gal4-UAS-Milton-RNAi*^{44477}*; Mito-GFP*, total number of mitochondrial movements=18, anterograde=12 and retrograde=6. (J) In *UAS-miro-RNAi*^{106683}*; Mito-GFP*, total number of mitochondrial movements=38, anterograde=38 and retrograde=0. See also Movies 3-6. Live imaging was performed under similar conditions, except for *milton-RNAi* where time frame was increased in order to visualize more mitochondrial movement (e.g. for all of the phenotypes frames were taken every 2 s for 5 min and for *milton-RNAi* frames were taken every 5 s for 12 min). Scale bars: 10 µm (A-D,F); 20 µm (E).

development in the wild type (i.e. 32 h APF), mitochondria were evenly distributed within the bristle shaft (Fig. 6B). In contrast, mitochondria were completely absent from the bristle shaft in *milton-RNAi* flies (Fig. 6B′). Later in development (i.e. 36-39 h APF), a small amount of unequally distributed mitochondria could be detected within the bristle shafts of the mutant flies (Fig. 6C′,D′). Since it was shown that Milton may interact with Dynein in sorting mitochondria into dendrites (van Spronsen et al., 2013), we tested

Development (2016) 143, 4203-4213 doi:10.1242/dev.138289

Table 1. Mitochondrial transport parameters in *Drosophila* bristles

	Wild type (*N*=7; *n*=7)		*Glued-DN* (*N*=5; *n*=10)		*milton-RNAi* (*N*=6; *n*=12)		*miro-RNAi* (*N*=5; *n*=11)	
	Anterograde	Retrograde	Anterograde	Retrograde	Anterograde	Retrograde	Anterograde	Retrograde
No. of moving mitochondria	163	57	238	26	120	44	288	22
Directionality proportion (%)	74±5	26±2	88.06±15.25*	11.94±15.25*	72.34±18.92	27.66±18.92	92.28±6.81*	7.72±6.81*
Velocity (μm/s)	2.04±1.06	2.08±0.19	2.39±2.32	2.18±1.66	2.45±1.66	2.21±1.46	2.09±1.36	1.45±0.54
Flux	2.39±1.45	0.92±0.68	2.74±1.84	0.24±0.29*	1.00±0.85*	0.38±0.34*	2.68±1.19	0.19±0.16*

The leading moving edge of each mitochondrion was marked in every frame of each movie taken from animals of each genotype. Directionality proportions, velocity and flux values reflect mean±s.d. Mutant parameters found to be significantly different from those of the wild type by nested ANOVA followed by a *post hoc* Tukey test (P<0.001) are marked with an asterisk. *N*, number of pupae; *n*, number of bristles.

whether mitochondrial distribution was likewise altered during bristle development in *Dhc64C* flies. We found no defects in mitochondrial distribution during development in *Dhc64C* flies (Fig. 6B″,C″,D″). Next, we quantified mitochondrial transport parameters in *milton-RNAi* mutant fly bristles (Movie 5) and found no significant difference in mitochondrial net velocity (Table 1; anterograde velocity, 2.45±1.66 and retrograde, 2.21±1.46 μm/s). Unexpectedly, we found no significant defects in the proportion of directional movement (anterograde: 72.34±18.92%; retrograde: 27.66±18.92; Fig. 5I), compared with the wild type (Movie 3). However, we did detect a significant reduction in both anterograde (1.00±0.85; P=0.009) and retrograde (0.38±0.34; P=0.0063) mitochondrial flux, compared with that in wild-type flies (Table 1). Thus, both the temporal delays in mitochondrial entry into the developing cell and the overall flux decreases observed suggest that Milton is involved in the early initiation of mitochondrial transport or is responsible for the polarized sorting of mitochondria.

Miro is required for retrograde motility of mitochondria during bristle development

It is broadly accepted that the protein Milton functions together with a second protein, Miro, to regulate mitochondrial transport (reviewed in Schwarz, 2013). As we found that Milton is required for sorting mitochondria into the bristle shaft, we now tested whether this function also required Miro. Accordingly, we first tested whether mutations in *miro* affected bristle development. Examination of bristle morphology from $dMiro^{B682}/dMiro^{Sd32}$

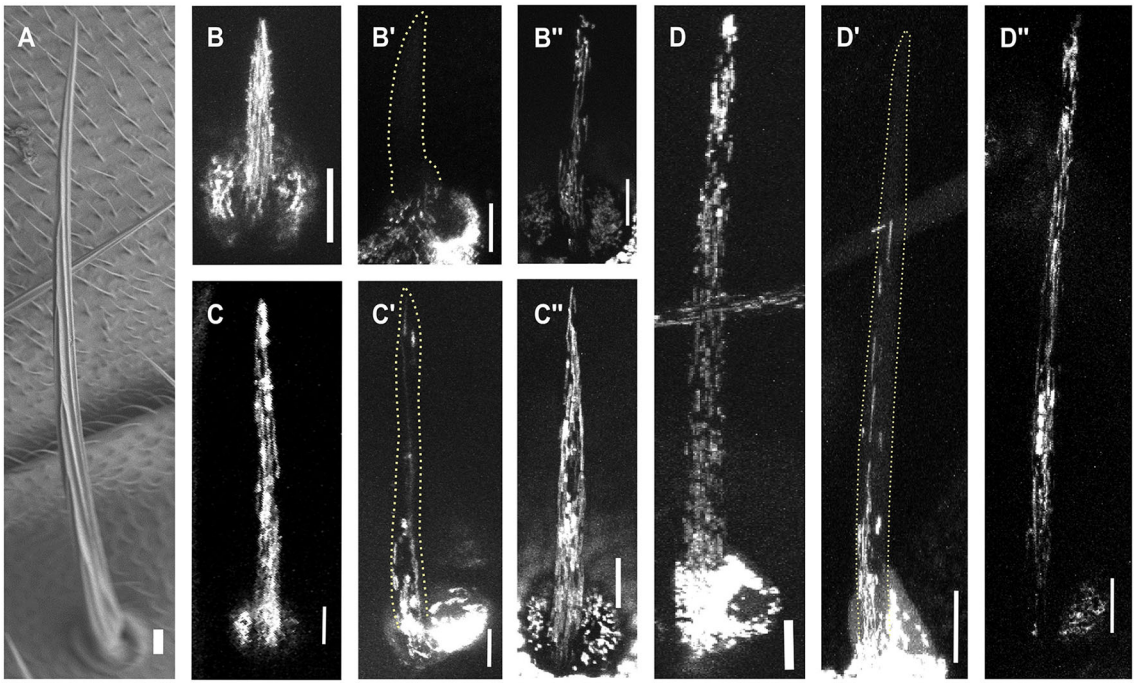

Fig. 6. Mutations in *milton* affect anterograde mitochondrial mobility. (A) SEM of adult bristle from *neur-Gal4-UAS-Milton-RNAi*^{44477} flies shows no detectable morphological defects. For comparison with the same region in wild-type flies, see Fig. 5A. (B) Confocal projection from a developing bristle expressing *UAS-Mito-GFP* from wild-type flies, ∼32 h APF. The young bristle cell at the beginning of the elongation process already fulfilled with mitochondria is seen. (B′) An elongating bristle from *neur-Gal4-UAS-Milton-RNAi*^{44477} flies at ∼32 h APF shows a lack of mitochondria inside the developing young bristle. The yellow dashed line here and in the following images marks the border of the cell. (B″) Confocal projection from the bristle from $Dhc64C^{8\text{-}1}/Dhc64C^{4\text{-}19}$ flies ∼32 h APF shows no obvious defects in mitochondrial distribution. (C) Confocal projection from a wild-type bristle at ∼36 h APF shows a dense mitochondria network filling the cell. (C′) Confocal projection from an elongating bristle from a *neur-Gal4-UAS-Milton-RNAi*^{44477} at ∼36 h APF shows decreased mitochondria density. (C″) Confocal projection from the elongating bristle from a $Dhc64C^{8\text{-}1}/Dhc64C^{4\text{-}19}$ fly ∼36 h APF shows a pattern similar to wild-type mitochondrial distribution. (D) Confocal projection from a wild-type bristle at ∼39 h APF, with the cell at an advanced elongation stage still showing mitochondria evenly distributed from the base to the tip, in contrast to what was seen in *neur-Gal4-UAS-Milton-RNAi*^{44477} flies at the same developmental stage (D′), demonstrating defective mitochondrial distribution and delayed mitochondria entry into the elongating bristle. (D″) Confocal projection from a $Dhc64C^{8\text{-}1}/Dhc64C^{4\text{-}19}$ bristle at ∼39 h APF shows no detectable defects in the mitochondrial localization pattern. Scale bars: 10 μm.

Development (2016) 143, 4203-4213 doi:10.1242/dev.138289

transheterozygotes, which died at late pupal stage before eclosion, revealed no significant phenotypic defects, with overall bristle length being normal (Fig. 7B,C). Indeed, only mild structural cuticular morphological aberrations were found in all tested bristles, with the characteristic parallel ridge surface morphology being affected in the middle part of the bristle (Fig. 7C; 16 bristles from 4 adult flies). We also downregulated *miro* levels in the bristles using *Miro-RNAi*^{106683} and found, as in the mutants, no defects in bristle lengths (Fig. 7D), although a slightly disrupted cuticular surface in the upper bristle regions was noted in all tested bristles (Fig. 7E; 16 bristles from 4 adult flies). Since there was a difference between the *miro* transheterozygote and *Miro-RNAi*^{106683} knockdown adult bristle phenotypes, we used a second RNAi line (*UAS-Miro-RNAi*^{iai}; Iijima-Ando et al., 2012) to confirm that the cuticular phenotype in *Miro-RNAi*^{106683} was indeed due to a loss of Miro and not the result of off-target effects. We found that downregulation of *miro* levels in the bristle using *UAS-Miro-RNAi*^{iai} (15 bristles from 6 adult flies; Fig. 7F,G) led to the identical cuticular phenotype as seen in the *Miro-RNAi*^{106683} flies (Fig. 7G). Next, we examined mitochondrial distribution in *Miro-RNAi*^{106683} flies and found that in contrast to the Milton-dependent mitochondrial phenotype, *Miro-RNAi*^{106683} flies presented no defects in mitochondrial distribution (Fig. 7H, Movie 6). Moreover, no obvious defects in MTs or actin organization were seen in the bristles of *Miro-RNAi*^{106683} flies (Fig. S1G-I). Next, we measured mitochondrial movement in *Miro-RNAi*^{106683} flies (Table 1 and Movie 6) and found no significant differences in either the anterograde (−2.09±1.36 µm/s) or retrograde (−1.45±0.54 µm/s) direction compared with the wild type. However, we detected a significant reduction (P<0.001) in retrograde (−0.19±0.16) but not anterograde mitochondrial flux (−2.68±1.19). Finally, a significant reduction (P=0.032) in the proportion of the retrograde-moving mitochondria was found in *Miro-RNAi*^{106683} (−7.72±6.81%) (Table 1 and Fig. 5J). Similar defects in mitochondria directionality and flux measurement were also detected using *UAS-Miro-RNAi*^{iai} (Table S1).

DISCUSSION

Dynein is the primary motor in both anterograde and retrograde bristle mitochondrial transport

Long-distance mitochondrial transport occurs mainly on MTs and is promoted by motor proteins. It was shown that kinesin and dynein motors drive mitochondrial transport in a manner reflecting microtubule polarity (reviewed in Schwarz, 2013). Accordingly, we found that whereas mutation in *Dhc64C* significantly reduced mitochondrial net velocity in both the antero- and the retrograde directions, mutations in *Khc* enhanced such velocities. These results further suggested that dynein is the primary motor for anterograde and retrograde bristle mitochondrial transport. In the current study, we provided additional evidence for the direct role of dynein in bristle mitochondrial transport by biochemically characterizing the effects of a mutation found in *Dhc64C*$^{8-1}$ allele that was used in our previous study. We first identified the molecular lesion in the *Dhc64C*$^{8-1}$ allele and localized it to the first AAA+ domain. Among the six AAA+ domains in the protein, hydrolysis in the first such domain mainly provided the energy needed for dynein motility. The affected residue corresponds to D1933 in human DYNC1H1, and is found in the loop between β-strand S2 and helix H2 in the luminal-facing potion of the AAA+ domain. In an MT-gliding assay using fully recombinant wild-type human dynein complex and mutant dynein complex (DYNC1H1$^{D/V}$), we demonstrated that this

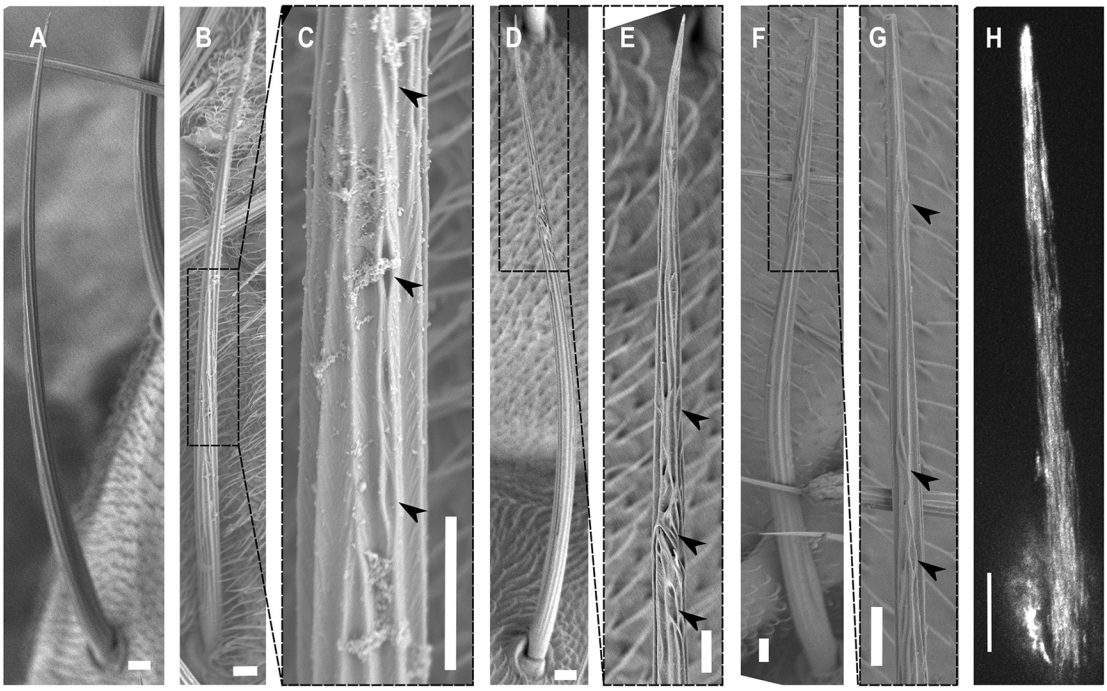

Fig. 7. Mutations in *miro* affect bristle morphology. Scanning electron micrographs of adult bristles from (A) wild-type flies; (B) *dMiro*^{B682}/*dMiro*^{Sd32} flies; (C) *dmiro*^{B682}/*dmiro*^{Sd32} flies showing higher magnification of the middle part of the bristle shaft with a mildly disrupted grooved surface marked by arrowheads; (D) *UAS-miro-RNAi*^{106683} flies, revealing defects similar to those of *miro* alleles; (E) *neur-Gal4-UAS-Miro-RNAi*^{106683} flies showing higher magnification of the tip area, reveal abnormal surface groove organization marked by arrowheads. (F) *UAS-Miro-RNAi*^{iai} bristle demonstrating defects in external cuticular morphology similar to previous RNAi strain. (G) Higher magnification of the bristle tip area showing the phenotypic abnormalities highlighted by arrowheads. (H) Confocal projection from *neur-Gal4-UAS-miro-RNAi*^{106683} flies showing a developing bristle expressing *UAS-mito-GFP*. No visible defects in mitochondrial distribution are seen. For comparison with the same region in wild-type flies, see Fig. 5E. Scale bars: 10 µm.

Development (2016) 143, 4203-4213 doi:10.1242/dev.138289

mutation significantly reduced MT-gliding activity, similar to the reduction in bristle mitochondrial net velocity found in our previous study (Melkov et al., 2015). Thus, our genetic and biochemical characterization revealed that the protein encoded by *Dhc64C*$^{8\text{-}1}$ is a 'slow' dynein mutant. The fact that this variant is a 'slow' dynein mutant, along with our finding that the net velocity of mitochondrial transport in both anterograde and retrograde directions is highly reduced in the presence of this allele (Melkov et al., 2015), provides further support for the notion that Dhc64C directly regulates anterograde and retrograde mitochondrial transport along the bristle shaft.

Dhc64C bristle phenotypes are probably not due to defects in mitochondrial transport

Previously, it was shown that mutations connected to mitochondrial function affect bristle morphology, resulting in the appearance of short and thin bristles (Mourikis et al., 2006). Our analysis of the defects in mitochondrial transport in *Dhc64C* bristle cells led us to further investigate the nature of the defects in the bristles of such mutants. We demonstrated that mutations in *Dhc64C* resulted in the production of shorter and thinner bristles (at least in the upper part of the shaft). Moreover, we found that both actin bundles and MT networks were dramatically disorganized in flies containing the mutant alleles. We found that more than 50% of the bristles presented defects in their growth direction. We also found that bristle morphology was strongly affected in *Glued-RNAi* and *Glued-DN* flies but surprisingly, no internal MT or actin organization defects were detected. However, examination of mitochondrial transport in *Glued* mutant bristles revealed that, in contrast to *Dhc64C*, this gene is not involved in the control of the mitochondrial velocity but rather serves a role in mitochondrial retrograde sorting. Examination of *miro* mutant bristles, the product of which is also involved in mitochondrial retrograde sorting, showed only mild bristle morphology defects. Unexpectedly, we found that in *milton-RNAi* mutant flies, where mitochondrial distribution in the shaft is severely affected as a result of defects in polarized sorting into the bristle shaft, wild type-like bristles were observed. It was also shown that although mitochondria were absent in axons and synapses in *milton* mutants, these structures presented normal general architecture, possessing microtubules, synaptic vesicles and active zone specializations (Gorska-Andrzejak et al., 2003; Stowers et al., 2002). Since affecting the mitochondria sorting machinery has little or no effect on bristle morphology, it would thus appear that the observed defects in *Dhc64C* bristle mutants are probably not due to defects in mitochondrial transport. Proper mitochondrial function, rather than mitochondrial transport or sorting, is crucial for the normal cell elongation process.

milton and *miro* play different roles in mitochondrial sorting

Transport of mitochondria in neurons, and possibly in most animal cells, requires a motor/adaptor complex (Brickley et al., 2005; Brickley and Stephenson, 2011; Fransson et al., 2003; Glater et al., 2006; Guo et al., 2005; Stowers et al., 2002). The core of this complex consists of three proteins, namely Khc, Miro and Milton. Recently, it was shown that dynein also interacts with Milton and Miro (van Spronsen et al., 2013). Milton was first identified as a protein that is required for *Drosophila* axonal transport of mitochondria to synapses (Stowers et al., 2002). Miro, an atypical mitochondrial GTPase (Fransson et al., 2003), was later identified as being encoded by a distinct gene in *Drosophila* associated with mitochondrial transport in axons (Guo et al., 2005). Later, it was shown that Milton and Miro form a protein complex that directly binds Khc to mitochondria (Glater et al., 2006). The mechanism by which Milton-Miro regulates mitochondrial mobility is by the binding of Khc to Miro via Milton to activate this complex in a Ca^{+2}-dependent manner, although the binding of Miro directly to Khc inactivates the motor by preventing its binding to MTs (Wang and Schwarz, 2009). Recently, it was shown the mammalian Milton homologs TRAK1 and TRAK2 steer mitochondrial transport into axons and dendrites by regulating both Khc and dynein motor proteins (van Spronsen et al., 2013). In the present study, we have shown for the first time that Milton and Miro assume different roles in regulating mitochondrial bristle transport. We found that mutations in these genes have different effects on mitochondrial transport. Whereas in *milton-RNAi*, mitochondria failed to enter the bristle shaft and presented defects in their anterograde mobility, upon introduction of *miro* RNAi, retrograde mitochondrial transport was severely affected. Based on our results, we suggest that dynein serves as the primary motor for mitochondrial bristle transport, and that *milton* and *miro* are not required for mitochondrial transport per se but rather regulate mitochondrial polarized sorting, with *milton* being required for anterograde transport and *miro* being needed for retrograde mobility.

MATERIALS AND METHODS

Drosophila stocks

Oregon-R was used as a wild-type control. The following mutant and transgenic flies were used: *Dhc64C*$^{4\text{-}19}$*/TM6B*, *Dhc64C*$^{8\text{-}1}$*/TM6B*, *Dhc64C*$^{3\text{-}2}$*/TM6B*, *Dhc64C*$^{6\text{-}6}$*/TM6B*, *Dhc64C*$^{6\text{-}10}$*/TM6B* (Gepner et al., 1996), *FRT79D Dhc64C*^{902}*/TM6B* (Li et al., 2008), *UAS-mito-HA-GFP* (Pilling et al., 2006), *Df-64B13-64C4/TM6B* (Bloomington, #7581), *UAS-Milton-RNAi* (Bloomington, #44477), *UAS-p150-delta96B* (Bloomington, #51645), *UAS-p150-RNAi* (Bloomington, #24760), *UAS-Miro-RNAi*^{106683} (Vienna *Drosophila* RNAi Center, #106683), *UAS-Miro-RNAi*^{iai} (Iijima-Ando et al., 2012), *dMiro*^{B682} and *dMiro*^{Sd32} (Guo et al., 2005). Bristle expression was induced under the control of the *neur-Gal4* or *sca-Gal4* driver.

Dissection and preparation of pupae for live imaging

After removing the pupal case, the pupae were dissected as previously described (Tilney et al., 1998; Melkov et al., 2015).

Bristle Phalloidin and antibody staining

The procedures used for fixation and staining were described previously (Guild et al., 2003; Melkov et al., 2015). Confocal images were taken using an Olympus FV1000 laser scanning confocal microscope and are shown here as *z*-projections in a few optical frames that together covered the bristle cell. Primary antibodies used were anti-acetylated tubulin mouse monoclonal antibodies (1:250; Sigma, T7451) and anti-Dyl (Dusky-like) rabbit polyclonal antibodies (1:250) (Fernandes et al., 2010). Cy3-conjugated goat anti-mouse (1:100; Jackson ImmunoResearch) and Alexa Fluor 488-conjugated goat anti-rabbit (1:100; Molecular Probes) secondary antibodies were used. For actin staining, we used Oregon Green 488- or Alexa Fluor 568-conjugated Phalloidin (1:250; Molecular Probes).

Transmission and scanning electron microscopy sample preparation

Pupae were dissected and prepared for transmission electron microscopy, as previously described (Melkov et al., 2015). The slices were stained with uranyl acetate and lead citrate and visualized with a JEM 1230 (JEOL) transmission electron microscope at 120 kV.

Adult *Drosophila* species of appropriate genotype were prepared for scanning electron microscopy as described in Melkov et al. (2015) and examined using a JEOL JSM-5610LV. Bristle length was measured using ImageJ software. Differences in bristle length between wild type and *Dhc64C* mutant were analyzed using nested ANOVA tests in which individual bristles (random factor) were nested within genotype (fixed factor). Whereas in *Dhc64C* and *miro* mutants all bristles were analyzed, in

Development (2016) 143, 4203-4213 doi:10.1242/dev.138289

UAS/Gal4-derived mutants, only the anterior and posterior scutellar bristles were used for SEM analysis.

Mitochondrial movement parameters and statistical analysis

Live imaging movies of bristle cells were recorded as previously described in Melkov et al. (2015). Tracking of mitochondria was manually performed using ImageJ software to measure the duration, start and end points of each mitochondria track. The collected data were analyzed using MATLAB R2010b (MathWorks). Mitochondrial flux was measured as normalized values of the number of mitochondria movements per 100 s to 100 μm^2. Differences between genotypes in antero- and retrograde flux were tested using one-way ANOVA, followed by a *post hoc* Tukey test. Flux was square-root transformed to correct for the deviation from normality. Mitochondria transport parameters (i.e. the proportion of anterograde and retrograde movement and movement velocity) were defined and analyzed as in Melkov et al. (2015). Velocity was log transformed and an angular transformation $[\arcsin(\sqrt[2]{P})]$ was applied for the proportion of movement.

Sequencing of mutant *Dhc64C* alleles

Genomic DNA was prepared from flies of the genotype *Dhc64C*/Df* according to standard procedures (Sambrook et al., 1989). The coding region was sequenced and the sequences of all three alleles were compared, since all alleles came from the same EMS screen (Qiu et al., 2012).

Recombinant human dynein expression and purification

We used site-directed mutagenesis to introduce point mutations into human DYNC1H1 (changing aspartic acid at 1933 to valine; called $DYNC1H1^{D/V}$). This mutation corresponds to the product of the $Dhc64C^{g-1}$ allele (D1922V). Expression and purification of wild-type and mutant dynein complex recombinant proteins was conducted as described (Schlager et al., 2014). SDS-PAGE was performed using Novex 4-12% Bis-Tris pre-cast gels using either MOPS or MES buffer (Life Technologies). Three independent rounds of expression and purification of wild-type and mutant dynein were conducted.

Microtubule-gliding assay

Microtubule-gliding assays were performed by attaching dynein via the introduced GFP tag to glass surfaces coated with anti-GFP antibodies (~400 µg/ml), as described previously (Reck-Peterson et al., 2006). Velocities of gliding microtubules were determined by manual analysis with Fiji software (http://fiji.sc/Fiji). From each purification, three independent MT-gliding assays were conducted. Differences in MT-gliding velocities between wild-type and $DYNC1H1^{D/V}$ samples were analyzed using nested ANOVA tests in which each movie (random factor) was nested within genotype (fixed factor). MT-gliding velocity was logarithmically transformed to correct for the skewed distribution of the data.

Acknowledgements

The MT-gliding assays were performed at Andrew Carter's lab and we would like to thank him for his generous support, advice and help. We thank Thomas Hays, Koichi Iijima, VDRC Austria, and the Bloomington Stock Center for generously providing fly strains, and Rina Jeger for her microtome expertise.

Competing interests

The authors declare no competing or financial interests.

Author contributions

A.M. designed the study, performed the experiments, analyzed the data and wrote the paper. R.B. performed the experiments, Y.A. analyzed the data. U.A. conceived and supervised the study, performed the experiments, analyzed the data and wrote the paper.

Funding

This research was supported by the Israel Science Foundation (278/16 to U.A.).

Data availability

Supplementary information

Supplementary information available online at
http://dev.biologists.org/lookup/doi/10.1242/dev.138289.supplemental

References

Allen, M. J., Shan, X., Caruccio, P., Froggett, S. J., Moffat, K. G. and Murphey, R. K. (1999). Targeted expression of truncated glued disrupts giant fiber synapse formation in Drosophila. *J. Neurosci.* **19**, 9374-9384.

Baas, P. W., Deitch, J. S., Black, M. M. and Banker, G. A. (1988). Polarity orientation of microtubules in hippocampal neurons: uniformity in the axon and nonuniformity in the dendrite. *Proc. Natl. Acad. Sci. USA* **85**, 8335-8339.

Bielska, E., Schuster, M., Roger, Y., Berepiki, A., Soanes, D. M., Talbot, N. J. and Steinberg, G. (2014). Hook is an adapter that coordinates kinesin-3 and dynein cargo attachment on early endosomes. *J. Cell Biol.* **204**, 989-1007.

Bitan, A., Rosenbaum, I. and Abdu, U. (2012). Stable and dynamic microtubules coordinately determine and maintain Drosophila bristle shape. *Development* **139**, 1987-1996.

Brickley, K. and Stephenson, F. A. (2011). Trafficking kinesin protein (TRAK)-mediated transport of mitochondria in axons of hippocampal neurons. *J. Biol. Chem.* **286**, 18079-18092.

Brickley, K., Smith, M. J., Beck, M. and Stephenson, F. A. (2005). GRIF-1 and OIP106, members of a novel gene family of coiled-coil domain proteins: association in vivo and in vitro with kinesin. *J. Biol. Chem.* **280**, 14723-14732.

Fernandes, I., Chanut-Delalande, H., Ferrer, P., Latapie, Y., Waltzer, L., Affolter, M., Payre, F. and Plaza, S. (2010). Zona pellucida domain proteins remodel the apical compartment for localized cell shape changes. *Dev. Cell* **18**, 64-76.

Fransson, A., Ruusala, A. and Aspenstrom, P. (2003). Atypical Rho GTPases have roles in mitochondrial homeostasis and apoptosis. *J. Biol. Chem.* **278**, 6495-6502.

Fransson, S., Ruusala, A. and Aspenstrom, P. (2006). The atypical Rho GTPases Miro-1 and Miro-2 have essential roles in mitochondrial trafficking. *Biochem. Biophys. Res. Commun.* **344**, 500-510.

Gepner, J., Li, M., Ludmann, S., Kortas, C., Boylan, K., Iyadurai, S. J., McGrail, M. and Hays, T. S. (1996). Cytoplasmic dynein function is essential in Drosophila melanogaster. *Genetics* **142**, 865-878.

Gill, S. R., Schroer, T. A., Szilak, I., Steuer, E. R., Sheetz, M. P. and Cleveland, D. W. (1991). Dynactin, a conserved, ubiquitously expressed component of an activator of vesicle motility mediated by cytoplasmic dynein. *J. Cell Biol.* **115**, 1639-1650.

Glater, E. E., Megeath, L. J., Stowers, R. S. and Schwarz, T. L. (2006). Axonal transport of mitochondria requires milton to recruit kinesin heavy chain and is light chain independent. *J. Cell Biol.* **173**, 545-557.

Gorska-Andrzejak, J., Stowers, R. S., Borycz, J., Kostyleva, R., Schwarz, T. L. and Meinertzhagen, I. A. (2003). Mitochondria are redistributed in Drosophila photoreceptors lacking milton, a kinesin-associated protein. *J. Comp. Neurol.* **463**, 372-388.

Guild, G. M., Connelly, P. S., Ruggiero, L., Vranich, K. A. and Tilney, L. G. (2003). Long continuous actin bundles in Drosophila bristles are constructed by overlapping short filaments. *J. Cell Biol.* **162**, 1069-1077.

Guo, X., Macleod, G. T., Wellington, A., Hu, F., Panchumarthi, S., Schoenfield, M., Marin, L., Charlton, M. P., Atwood, H. L. and Zinsmaier, K. E. (2005). The GTPase dMiro is required for axonal transport of mitochondria to Drosophila synapses. *Neuron* **47**, 379-393.

Holzbaur, E. L., Hammarback, J. A., Paschal, B. M., Kravit, N. G., Pfister, K. K. and Vallee, R. B. (1991). Homology of a 150K cytoplasmic dynein-associated polypeptide with the Drosophila gene Glued. *Nature* **351**, 579-583.

Horne-Badovinac, S. and Bilder, D. (2008). Dynein regulates epithelial polarity and the apical localization of stardust A mRNA. *PLoS Genet.* **4**, e8.

Iijima-Ando, K., Sekiya, M., Maruko-Otake, A., Ohtake, Y., Suzuki, E., Lu, B. and Iijima, K. M. (2012). Loss of axonal mitochondria promotes Tau-mediated neurodegeneration and Alzheimer's disease-related Tau phosphorylation via PAR-1. *PLoS Genet.* **8**, e1002918.

Kardon, J. R. and Vale, R. D. (2009). Regulators of the cytoplasmic dynein motor. *Nat Rev Mol Cell Biol.* **10**, 854-65.

Kikkawa, M. (2013). Big steps toward understanding dynein. *J. Cell Biol.* **202**, 15-23.

Koutsopoulos, O. S., Laine, D., Osellame, L., Chudakov, D. M., Parton, R. G., Frazier, A. E. and Ryan, M. T. (2010). Human Miltons associate with mitochondria and induce microtubule-dependent remodeling of mitochondrial networks. *Biochim. Biophys. Acta* **1803**, 564-574.

Li, Z., Wang, L., Hays, T. S. and Cai, Y. (2008). Dynein-mediated apical localization of crumbs transcripts is required for Crumbs activity in epithelial polarity. *J. Cell Biol.* **180**, 31-38.

Macaskill, A. F., Rinholm, J. E., Twelvetrees, A. E., Arancibia-Carcamo, I. L., Muir, J., Fransson, A., Aspenstrom, P., Attwell, D. and Kittler, J. T. (2009). Miro1 is a calcium sensor for glutamate receptor-dependent localization of mitochondria at synapses. *Neuron* **61**, 541-555.

Melkov, A., Simchoni, Y., Alcalay, Y. and Abdu, U. (2015). Dynamic microtubule organization and mitochondrial transport are regulated by distinct Kinesin-1 pathways. *Biol. Open* **4**, 1696-1706.

Mourikis, P., Hurlbut, G. D. and Artavanis-Tsakonas, S. (2006). Enigma, a mitochondrial protein affecting lifespan and oxidative stress response in Drosophila. *Proc. Natl. Acad. Sci. USA* **103**, 1307-1312.

Nagaraj, R. and Adler, P. N. (2012). Dusky-like functions as a Rab11 effector for the deposition of cuticle during Drosophila bristle development. *Development* **139**, 906-916.
Pilling, A. D., Horiuchi, D., Lively, C. M. and Saxton, W. M. (2006). Kinesin-1 and Dynein are the primary motors for fast transport of mitochondria in Drosophila motor axons. *Mol. Biol. Cell* **17**, 2057-2068.
Qiu, W., Derr, N. D., Goodman, B. S., Villa, E., Wu, D., Shih, W. and Reck-Peterson, S. L. (2012). Dynein achieves processive motion using both stochastic and coordinated stepping. *Nat. Struct. Mol. Biol.* **19**, 193-200.
Reck-Peterson, S. L., Yildiz, A., Carter, A. P., Gennerich, A., Zhang, N. and Vale, R. D. (2006). Single-molecule analysis of dynein processivity and stepping behavior. *Cell* **126**, 335-348.
Sambrook, J., Fritsch, E. F. and Maniatis, T. (1989). *Molecular Cloning*, Vol. **2.** New York: Cold Spring Harbor Laboratory Press.
Saotome, M., Safiulina, D., Szabadkai, G., Das, S., Fransson, A., Aspenstrom, P., Rizzuto, R. and Hajnoczky, G. (2008). Bidirectional Ca2+-dependent control of mitochondrial dynamics by the Miro GTPase. *Proc. Natl. Acad. Sci. USA* **105**, 20728-20733.
Schlager, M. A., Hoang, H. T., Urnavicius, L., Bullock, S. L. and Carter, A. P. (2014). In vitro reconstitution of a highly processive recombinant human dynein complex. *EMBO J.* **33**, 1855-1868.
Schroer, T. A. (2004). Dynactin. *Annu Rev Cell Dev Biol.* **20**, 759-779.
Schwarz, T. L. (2013). Mitochondrial trafficking in neurons. *Cold Spring Harb. Perspect. Biol.* **5**, a011304.
Silvanovich, A., Li, M.-G., Serr, M., Mische, S. and Hays, T. S. (2003). The third P-loop domain in cytoplasmic dynein heavy chain is essential for dynein motor function and ATP-sensitive microtubule binding. *Mol. Biol. Cell* **14**, 1355-1365.
Stone, M. C., Roegiers, F. and Rolls, M. M. (2008). Microtubules have opposite orientation in axons and dendrites of Drosophila neurons. *Mol. Biol. Cell* **19**, 4122-4129.
Stowers, R. S., Megeath, L. J., Gorska-Andrzejak, J., Meinertzhagen, I. A. and Schwarz, T. L. (2002). Axonal transport of mitochondria to synapses depends on milton, a novel Drosophila protein. *Neuron* **36**, 1063-1077.
Swaroop, A., Swaroop, M. and Garen, A. (1987). Sequence analysis of the complete cDNA and encoded polypeptide for the Glued gene of *Drosophila melanogaster*. *Proc. Natl Acad. Sci. USA* **84**, 6501-6505.
Tilney, L. G., Connelly, P. S., Vranich, K. A., Shaw, M. K. and Guild, G. M. (1998). Why are two different cross-linkers necessary for actin bundle formation in vivo and what does each cross-link contribute? *J. Cell Biol.* **143**, 121-133.
Tilney, L. G., Connelly, P. S., Vranich, K. A., Shaw, M. K. and Guild, G. M. (2000). Actin filaments and microtubules play different roles during bristle elongation in Drosophila. *J. Cell Sci.* **113**, 1255-1265.
van Spronsen, M., Mikhaylova, M., Lipka, J., Schlager, M. A., van den Heuvel, D. J., Kuijpers, M., Wulf, P. S., Keijzer, N., Demmers, J. and Kapitein, L. C. (2013). TRAK/Milton motor-adaptor proteins steer mitochondrial trafficking to axons and dendrites. *Neuron* **77**, 485-502.
Wang, X. and Schwarz, T. L. (2009). The mechanism of Ca2+ -dependent regulation of kinesin-mediated mitochondrial motility. *Cell* **136**, 163-174.